MATER. RES. LETT.
2020, VOL. 8, NO. 11, 399–407
https://doi.org/10.1080/21663831.2020.1777215

MATERIALS RESEARCH LETTERS
Taylor & Francis
Taylor & Francis Group

ORIGINAL REPORT

Engineering transformation pathways in an $Al_{0.3}CoFeNi$ complex concentrated alloy leads to excellent strength–ductility combination

S. Dasari[a], A. Jagetia[a], V. Soni[a], B. Gwalani[a], S. Gorsse [b] and R. Banerjee[a]

[a]Department of Materials Science and Engineering, University of North Texas, Denton, TX, USA; [b]CNRS, Univ. Bordeaux, Bordeaux INP, ICMCB, UMR 5026, 33600 Pessac, France

ABSTRACT

Guided by thermodynamic modeling, engineering phase transformation pathways via thermo-mechanical processing, in a complex concentrated alloy/high entropy alloy (HEA) of composition $Al_{0.3}CoFeNi$, lead to a novel multi-scale microstructure consisting of fine-scale FCC + $L1_2$ grains mixed with B2 + BCC grains. The two-step pathway comprises initial decomposition of the parent single-phase FCC to form a fine-grained FCC + B2 microstructure, which further decomposes in the second step into the complex four-phase mixture, exhibiting an excellent combination of tensile yield stress of ~1490 MPa, ultimate tensile strength of ~1663 MPa, with a good ductility of ~12% at room temperature.

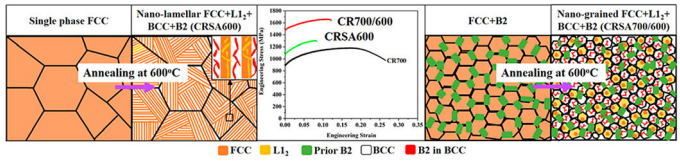

IMPACT STATEMENT

This paper reports a novel multi-phase microstructure in a HEA/CCA similar to the microstructure observed in dual-phase stainless steel. This report exemplifies the novelty of HEA/CCA compositional space.

ARTICLE HISTORY
Received 29 April 2020

KEYWORDS
High entropy alloys; complex concentrated alloys; multicomponent intermetallic precipitation; multi-phase microstructure; mechanical properties

Introduction

The conventional alloy design has produced a plethora of microstructures that have been proven beneficial in many structural applications [1]. However, starting from the single-phase solid solutions like Fe–C to pearlitic steels, alloy steels, simple precipitation hardenable alloys like Al–Cu to complex Fe/Co/Ni superalloys have largely been focused on the corners and edges of multicomponent phase diagrams. In contrast, the concept of high entropy alloys (HEAs) or complex concentrated alloys (CCAs), proposed about 15 years ago, offers the compositional space at the center of phase diagrams which has been far less explored [2,3]. The chemical combination of multiple elements which is central to the idea of HEA/CCAs enables exploitation of the competition between enthalpy and configurational entropy to achieve desired phase stability and design novel microstructures. Thus, despite the widely successful microstructures obtained with conventional alloys based on pearlite, martensite, $\gamma-\gamma'$ and other precipitate phases and micro-constituents, HEA/CCAs offer exciting opportunities for tuning phase stability and microstructure [4,5]. Over the past few years, there has been a rise in papers reporting HEA/CCAs with novel microstructures and excellent tunability in physical and mechanical properties [6–8].

The phase decomposition in the as-cast AlCoCrCuFeNi has been examined in detail by Singh et al. [9]. While the interdendritic regions consist of a Cu-rich $L1_2$ phase, the dendritic regions are composed of six different phases. The formation of such a complex microstructure has been attributed to the large differences in the enthalpy

CONTACT R. Banerjee raj.banerjee@unt.edu Department of Materials Science and Engineering, University of North Texas, Denton, TX 76207, USA
* Currently at Physical and Computational Sciences Directorate, Pacific Northwest National Laboratory, 902 Battelle Blvd, Richland, WA 99352, USA.

Supplemental data for this article can be accessed here. https://doi.org/10.1080/21663831.2020.1777215

of mixing between Al–Ni, Cu–Ni and Fe–Cr. Liang et al. [10] obtained a spinodally decomposed FCC + $L1_2$ microstructure in $Al_{0.5}Cr_{0.9}FeNi_{2.5}V_{0.2}$ HEA/CCA that exhibited a room temperature tensile yield strength of ~1.5 GPa and ~9% ductility. Soni et al. [11] reported the formation of multiple length scales of BCC within B2 and the B2 formation within BCC in the same microstructure. A BCC + B2 microstructure resembling the well-known $\gamma-\gamma'$ microstructure in Ni-based superalloys was reported for $Fe_{36}Mn_{21}Cr_{18}Ni_{15}Al_{10}$ [12]. High saturation magnetization and low coercivity were reported for a high strength HEA, $FeCoNiCu_{0.2}Si_{0.2}$, with a yield strength of ~820 MPa [13]. Nanostructured forms of the well-known HEA, CoCrFeMnNi, and a well-known medium entropy alloy, CoCrNi, were reported to exhibit creep resistances higher than conventional nanostructured metals [14]. Furthermore, it has also been proposed that HEA/CCAs exhibit deformation mechanisms that extend from conventional alloys to amorphous metals [15].

Duplex microstructures have also been reported with both conventional alloy and HEA/CCAs that possess excellent strength–ductility combinations. The duplex ferrite–austenite microstructures in stainless steels were often reported to have the best tensile yield strengths in the range of 750–850 MPa [16]. In HEA/CCAs, Gwalani et al. [17] reported a eutectic FCC + B2 dual-phase microstructure with $L1_2$ precipitation inside FCC lamella and BCC precipitation inside B2 lamella that exhibited a yield strength of ~990 MPa and ~13% ductility in tension. Shi et al. [18] reported a recrystallized grain structure and precipitation within the alternating FCC and B2 eutectic lamella of $AlCoCrFeNi_{2.1}$ HEA/CCA. This microstructure exhibited tensile yield stress of ~1.5 GPa and ~16% ductility. Nevertheless, the dual-phase microstructures reported so far in HEA/CCAs have largely been based on eutectic or precipitation reactions. Based on the idea of HEA/CCAs, multicomponent intermetallics have also been studied previously [19,20]. A six-component single-phase $L1_2$ alloy has been reported that possesses compressive yield strength of ~600 MPa and extraordinary strain hardening [20].

In this study, a novel FCC + $L1_2$ + BCC + B2 four-phase microstructure is being reported in a four-component HEA/CCA, $Al_{0.3}$CoFeNi, that brings together the ideas of complex multicomponent intermetallics coupled with multi-phase microstructures. A recent paper on the same $Al_{0.3}$CoFeNi CCA has reported an FCC + B2 microstructure at 700°C, and a complex nano-lamellar, eutectoid-like microstructure consisting of a four-phase mixture, FCC + $L1_2$ + BCC + B2 at 600°C [21]. However, the balance of mechanical properties reported for either of these conditions was not very attractive. Therefore, this paper focuses on engineering, the phase transformation pathways, to obtain a strikingly different microstructure in the $Al_{0.3}$CoFeNi CCA with the objective of enhancing the mechanical properties. Thermo-mechanical processing has been used to modify the supersaturation within the FCC solid solution at 700°C, to eventually suppress the formation of the nano-lamellar microstructure at 600°C. Detailed characterization of the microstructure was performed with TEM and mechanical properties were measured via room temperature tensile testing. CALPHAD modeling was done using ThermoCalc with the TCHEA4 database.

Materials and methods

$Al_{0.3}$CoFeNi, with the nominal chemical composition 9.1Al-30.3Co-30.3Fe-30.3Ni (at.%), was produced using conventional arc melting. The purity of individual elements used in the fabrication of the cast $Al_{0.3}$CoFeNi alloy is as follows: Al-99.9%, Co-99.9%, Fe-99.9% and Ni-99.9%. The cast alloy was homogenized at 1250°C for 30 min before rolling and annealing treatments. Three processing routes have been examined in this study, CR700 condition which involved single-step annealing treatment, CRSA600 which involved solution treatment and precipitation annealing, and CR700/600 condition which involved two-step annealing treatment. The homogenized alloy was cold-rolled to 85% and directly annealed either at 700°C for 50 h (CR700 condition) or 1200°C for 5 min followed by annealing at 600°C for 50 h (CRSA600 condition). In the case of CR700/600 condition, the rolled alloy was annealed at 700°C for 50 h followed by 600°C for 50 h. All samples were encapsulated in quartz tubes backfilled with argon for heat treatments and water quenching was used for the cooling process. The schematics for the three processing conditions are shown in Fig. S1. Microstructural characterization was performed with FEI Nova-NanoSEM 230™ scanning electron microscope (SEM) fixed with the Hikari Super electron backscattered diffraction (EBSD) detector and FEI Tecnai G2 TF20™ transmission electron microscopy (TEM) operating at 200 kV. TEM lift-outs were prepared using an FEI Nova 200 dual-beam focused ion beam (FIB) microscope. A TEM lift-out of dimensions ~15 × 2 × 5 μm was initially prepared with the help of the omniprobe micromanipulator in FIB. This 2 μm thick sample was subsequently thinned to dimensions ~50–100 nm in multiple steps by progressively reducing the voltage and/or current of the Ga ion beam in the dual-beam FIB. Mechanical properties were measured in a customized mini-tensile testing machine at a strain rate of 0.001/s, which used a linear variable

displacement transformer extensometer. Tensile specimens with approximate gauge dimensions 3 × 1 × 1 mm were sectioned in an electric discharge machine according to ASTM E8 standard. Three specimens were tested for each condition for statistical purposes.

Results and discussion

Using solution thermodynamic modeling (ThermoCalc with TCHEA4 database), an isopleth has been computed to depict changes in phase stability as a function of Al content (0–25 at.%) in the equi-atomic CoFeNi solid solution, as shown in Figure 1(a). With increasing Al content, the high-temperature FCC single-phase field transforms to a dual-phase FCC + B2 region, eventually becoming a single B2 phase for high Al contents (> 20 at.%). The composition $Al_{0.3}$CoFeNi marked by a dotted line in Figure 1(a) exhibits a wide FCC + B2 phase field at high temperatures and an FCC + $L1_2$+B2 phase field at low temperatures, based on the ThermoCalc prediction. Additionally, the existence of FCC single-phase field above ~ 1150°C allows for the thermomechanical processing of the alloy to exploit the ordering tendency introduced by Al [21]. The phase fraction vs. temperature plot for $Al_{0.3}$CoFeNi composition is shown in Figure 1(b). While the plot shows that the equilibrium phase composition is FCC + $L1_2$ + B2 at 600°C, the experimentally observed phase composition was FCC + $L1_2$ + BCC + B2 [21]. This could be attributed to the inaccuracies in solution thermodynamic modeling for these complex alloys.

The SEM backscatter micrograph given in Figure 2(a) shows the fully recrystallized dual-phase microstructure in CR700 condition. The high magnification picture in Figure 2(b) reveals fine FCC grains with a uniform distribution of B2 precipitates (dark contrast) which primarily appear to nucleate at grain boundaries and triple junctions. The microstructure in the CR700 condition is a result of precipitation of B2 concurrently with recrystallization of FCC grains, due to the availability of heterogenous nucleation sites like grain boundaries, triple junctions and deformation bands/twins, as discussed in detail in previous reports on direct annealing after cold-rolling of HEAs/CCAs [4,21]. Interestingly, the lower magnification micrographs of CR700/600 condition given in Figure 2(c, d), when compared with same magnification pictures of CR700 in Figure 2(a, b), reveals that while the FCC + B2 microstructure is retained, the grain structure appears to be relatively refined after annealing at 600°C. Additionally, multiple grains show further decomposition which can be seen in Figure 2(d). A high magnification picture from one such grain reveals that the intragranular phase has a network-like morphology

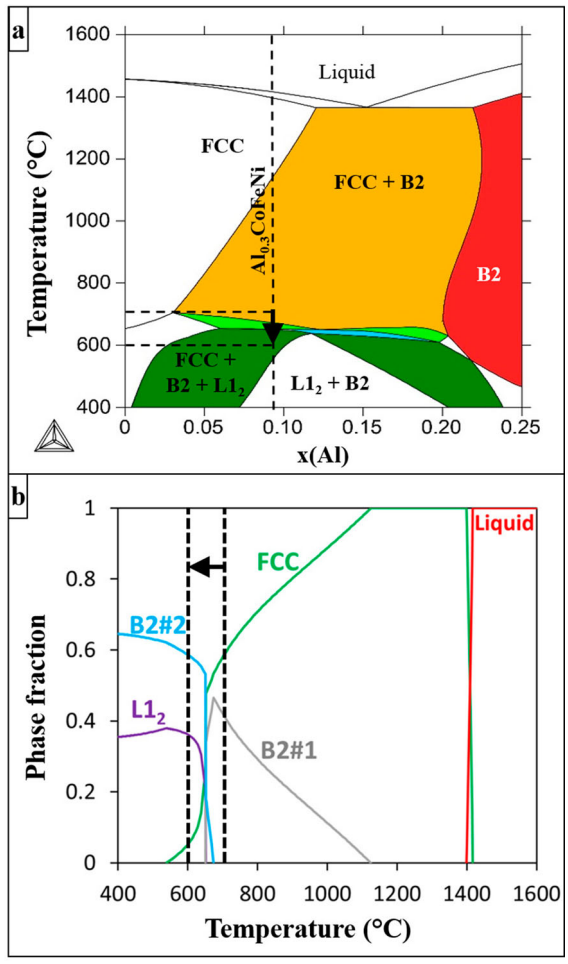

Figure 1. (a) Isopleth obtained by varying Al content in CoFeNi and (b) phase fraction vs. temperature plot for $Al_{0.3}$CoFeNi.

(Figure 2(e)). Figure 2(f) shows the microstructure of the same CCA in CRSA600 condition. This is a completely different microstructure consisting of multiple colonies of nano-lamellae that have developed within the FCC parent grains, comprising a four-phase mixture of FCC + $L1_2$ + BCC + B2, resulting from a eutectoid-like solid-state transformation [21]. This microstructure has been shown here to reveal the completely different decomposition pathway when this alloy is directly annealed at 600°C, starting from a single FCC phase.

Detailed characterization was performed using TEM to reveal the crystallographic identity of phases in case of the CR700/600 condition, after the second annealing step at 600°C. A bright-field image from a B2 precipitate is shown in Figure 3(a), and the [001] BCC zone axis diffraction pattern showing {001} superlattice reflections is shown as an inset, confirming its B2 crystal structure. The corresponding {001} superlattice dark-field micrograph is shown in Figure 3(b). A diffraction pattern recorded from one of the grains showing a network-like internal structure is shown as an inset in Figure 3(d),

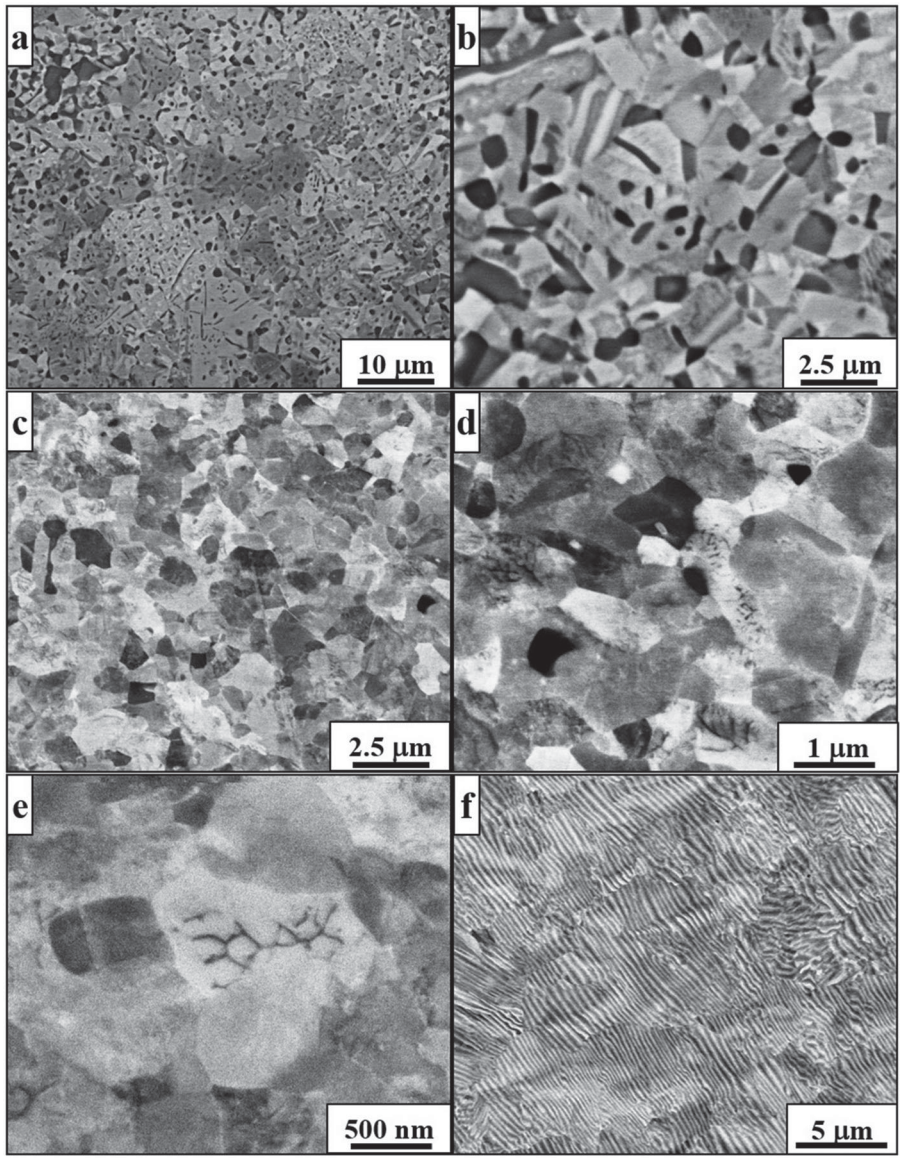

Figure 2. Backscatter SEM micrographs of (a, b) CR700 condition showing an FCC + B2 microstructure (B2 in dark contrast), (c–e) CR700/600 condition showing equiaxed ultrafine grains and further decomposition within the grains and (f) CRSA600 condition showing a nano-lamellar eutectoid-like microstructure.

and the corresponding bright-field and dark-field images in Figure 3(c, d). This diffraction pattern can be consistently indexed based on the [011] zone axis of a BCC phase with {001} B2 superlattice reflections. The dark-field micrograph from one of the {001} superlattice reflections reveals that the grain comprises a BCC matrix with a network-like B2 region (Figure 3(d)). The diffraction analysis from an FCC grain is shown in Figure 3(e, f). The bright-field micrograph and the corresponding [011] FCC zone axis diffraction pattern (inset) are shown in Figure 3(e). The superlattice reflections at {001} positions indicate the presence of the $L1_2$ phase, and a superlattice dark-field image is shown in Figure 3(f) revealing FCC domains within an ordered $L1_2$ matrix. STEM-EDS maps including an interphase boundary between FCC + $L1_2$ and BCC + B2 regions are shown in Figure 4. The majority area of these maps shows a BCC grain with an internal network-like structure. The enrichment of Fe and Co within the BCC grain and Ni and Al enrichment in the network-like B2 phase is clearly visible. An FCC + $L1_2$ grain has also been marked at the top of the map, which shows Ni + Al enrichment in the $L1_2$ region and Fe + Co enrichment (and Ni + Al depletion) in the FCC region. Thus, the microstructure in duplex aged condition contains four phases, and can be described as a mixture of (FCC + $L1_2$) grains together with B2 grains as well as (BCC + B2) grains. The schematics illustrating the phase transformation pathway have been shown in Fig. S2.

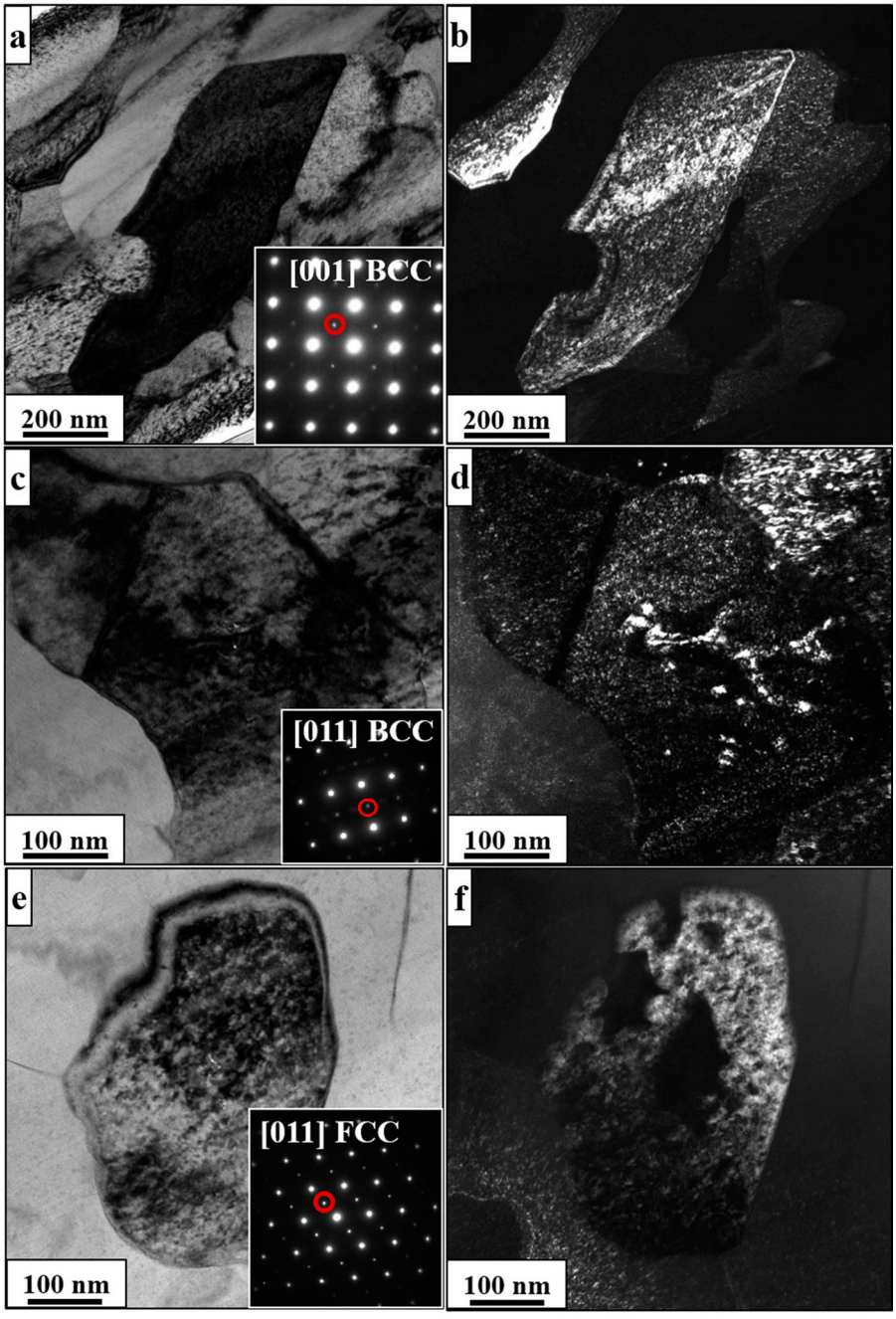

Figure 3. TEM of CR700/600 condition. (a) Bright-field (BF) and (b) dark-field (DF) micrographs of a B2 grain retained from prior annealing at 700°C. Diffraction pattern from [001] BCC is given in the inset of (a). (c) BF and (d) DF imaging of a BCC grain with network-like structure. Diffraction pattern from [011] BCC is given in the inset of (c). (e) BF and (f) DF images from an FCC grain. Diffraction pattern from [011] FCC is shown as an inset in (e).

However, the current microstructure in CR700/600 condition is in stark contrast to the pearlite-like nano-lamellar microstructure observed before. In the previous report [21], the supersaturated FCC solid solution was directly annealed at 600°C and it resulted in a eutectoid-like nano-lamellar microstructure with alternating FCC + $L1_2$ and BCC + B2 lamellae. The present study includes the first-step annealing at 700°C which results in a reduction of the supersaturation within the FCC matrix due to B2 precipitation. The equilibrium phase fraction and composition of B2 at 700°C, predicted by ThermoCalc, are 42% and 17Al-27.6Co-30.9 Fe-24.5Ni (at.%), respectively, as shown in Table 1. However, the experimentally observed B2 phase fraction after 700°C/50 h annealing is ~25% based on image analysis. This could be due to the slower kinetics of B2 growth which results in a higher Al and Ni supersaturation retained within the FCC matrix as compared to the

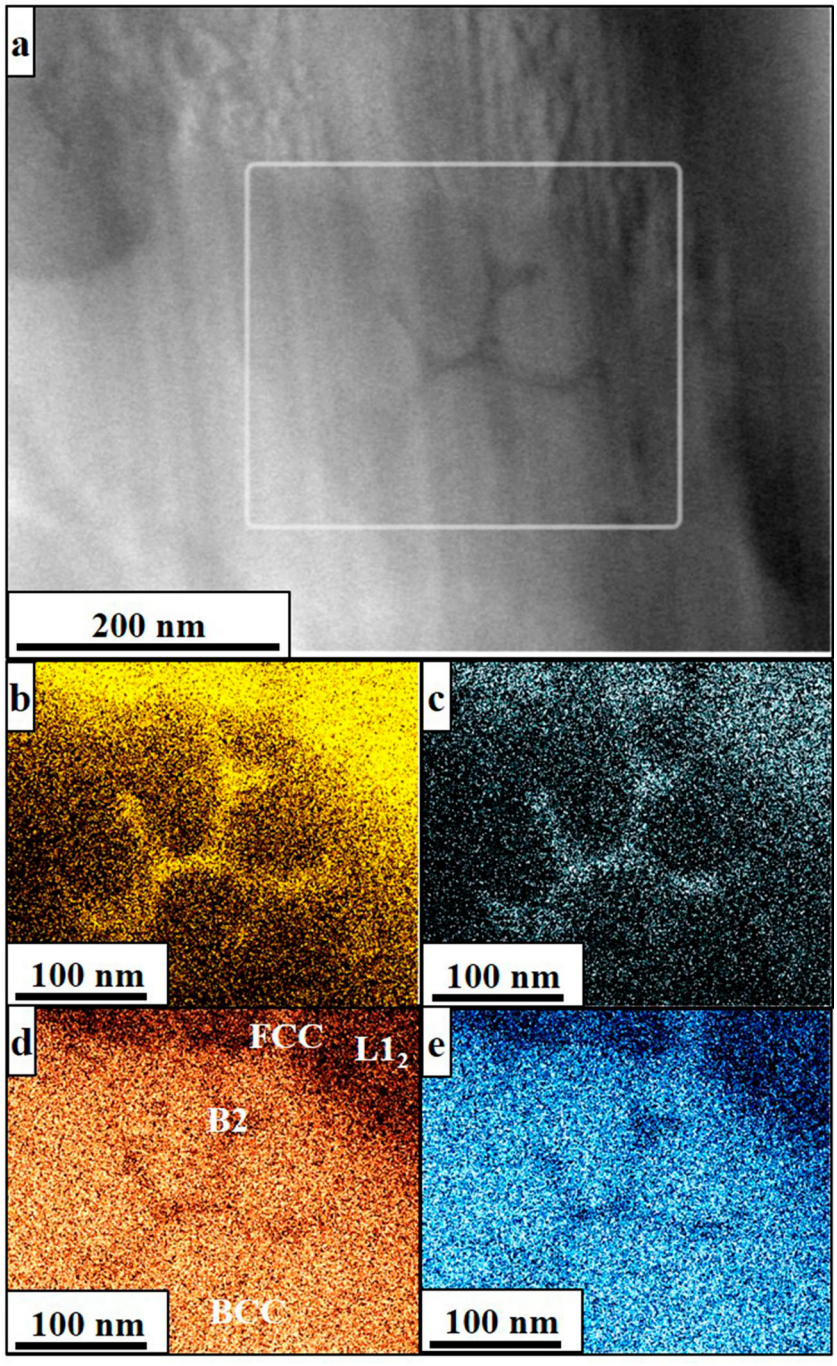

Figure 4. STEM-EDS mapping of CR700/600 condition. (a) STEM micrograph of a region with network-like B2 structure. The EDS mapping was done on the highlighted area. (b) Ni map, (c) Al map, (d) Fe map and (e) Co map.

equilibrium 3.4 at.% Al and 34.5 at.% Ni. Based on a phase fraction ~25% and an equilibrium composition for the B2 phase, the expected FCC matrix composition is 6.5Al-31.2Co-30.1Fe-32.3Ni (at.%). As reported previously, the decomposition of a supersaturated FCC solid solution with a nominal composition of $Al_{0.3}$CoFeNi results in a nano-lamellar (FCC + $L1_2$)/(BCC + B2) microstructure [21]. However, in case of the two-step CR700/600 condition, the FCC matrix composition (within the two-phase FCC + B2 mixture) inherited from the prior annealing at 700°C/50 h, is different from the nominal alloy composition. Consequently, the phase decomposition pathway within this retained FCC matrix changes at 600°C, as compared to the global equilibrium condition when a single FCC matrix decomposes at 600°C. ThermoCalc computations were employed to predict the decomposition products of this retained FCC phase, which are B2 and $L1_2$ phases, and their corresponding

Table 1. The equilibrium phase composition and phase fractions at 700°C for $Al_{0.3}CoFeNi$.

	Phase composition (at.%)				
Phase	Al	Co	Fe	Ni	Phase fraction
FCC	3.4	32.3	29.8	34.5	58%
B2	17.0	27.6	30.9	24.5	42%

Table 2. The equilibrium phase composition and phase fractions at 600°C calculated based on the expected FCC phase composition at 700°C.

	Phase composition (at.%)					
Phase	Al	Co	Fe	Ni	Phase fraction	Normalized onset driving force (/RT)
FCC	1.1	37.0	24.1	37.8	27%	-
B2	5.5	38.6	42.1	13.8	45%	0.49
$L1_2$	13.4	13.4	16.6	56.6	28%	0.18

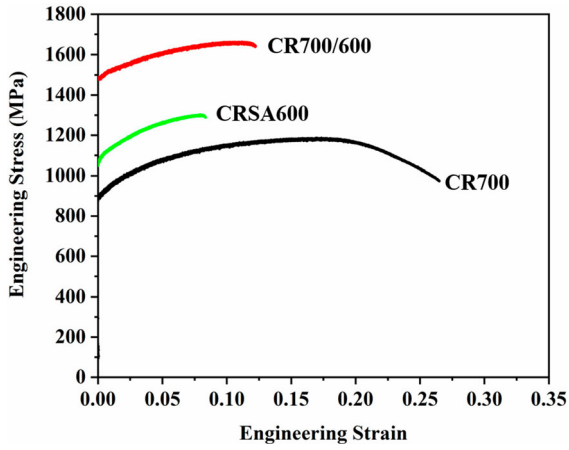

Figure 5. Tensile engineering stress–strain curves of CR700, CRSA600 and CR700/600 conditions.

onset driving forces, the results are shown in Table 2. The predicted B2 composition at 600°C is substantially leaner in Al and Ni content, and richer in Fe and Co content, as compared to the predicted B2 composition at 700°C (refer to Table 1). Stabilization of a single B2 phase with such a high Fe and Co content, and low Al and Ni content is unlikely, and is possibly the reason underlying the further decomposition of the B2 grains into BCC + B2 as observed experimentally (refer to Figure 3(c, d)). Based on the experimental observations and the ThermoCalc predictions, a transformation pathway can be predicted for the partially supersaturated FCC solid solution retained from the 700°C/50 h annealing treatment. Thus, when this FCC matrix is annealed at a lower temperature of 600°C, it starts transforming to FCC + $L1_2$ mixture with nearly equal fractions of both phases, rejecting Fe and Co. The rejected Fe and Co aids in the heterogeneous nucleation of new BCC precipitates (different from the pre-existing B2 precipitates from the 700°C/50 h annealing) at FCC grain boundaries or FCC/B2 interfaces. The growing BCC precipitates further internally decompose into Fe- and Co-rich BCC and Al- and Ni-rich B2 phases. This results in the observed microstructure consisting of (FCC + $L1_2$) grains together B2 grains as well as (BCC + B2) grains. The higher driving force and the higher equilibrium phase fraction of B2, predicted by ThermoCalc, indicate that BCC + B2 comprises the majority of the microstructure at 600°C. The predicted phase fraction of ∼55% (FCC + $L1_2$) and ∼45% (BCC + B2) is in reasonable agreement with the experimentally observed phase fractions of ∼45% (FCC + $L1_2$) and 55% (BCC + B2) obtained from EBSD. Thus, the phase transformation pathway has been modified from eutectoid/discontinuous precipitation to a two-step decomposition process resulting in this complex hierarchical four-phase microstructure.

The tensile engineering stress–strain curves of the CR700 and CR700/600 conditions, together with the CRSA600 condition are shown in Figure 5. The FCC + B2 dual-phase microstructure, in case of the CR700 condition, exhibits tensile yield stress of ∼900 MPa, ultimate tensile stress (UTS) of ∼1187 MPa and ∼26% ductility. The grain boundary or Hall-Petch strengthening from the fine-grained FCC matrix, coupled with the composite strengthening from B2 grains, results in a good balance of tensile properties for this condition. The complex nano-lamellar (FCC + $L1_2$)/(BCC + B2) microstructure reported previously for the CRSA600 condition [21] exhibits yield stress of ∼1074 MPa with ∼8% tensile ductility. While the higher strength can be attributed to constriction of dislocation glide within the ∼150 nm lamellae, the significant plastic strain could potentially be a result of interlamellar slip as observed in pearlite [22]. The hierarchical four-phase FCC + $L1_2$ + B2 + BCC microstructure in the CR700/600 condition, consisting of ∼1 μm grains, exhibits extraordinarily high yield stress ∼1490 MPa, UTS ∼1663 MPa and ∼12% tensile ductility. This excellent combination of tensile properties can potentially be attributed to the hierarchical four-phase microstructure, consisting of three distinct types of grains. These include FCC-based grains consisting of a nanoscale mixture of FCC and intermetallic L12 phases, single B2 phase intermetallic grains and BCC-based grains containing a mixture of BCC and intermetallic B2 phases. The improved ductility in the case of CR700/600 as compared to CRSA600 could possibly be attributed to a larger slip length in the former case [23]. In CRSA600, slip is essentially confined to ∼150 nm FCC/BCC lamellae and slip propagation between lamellae will be determined by the FCC/BCC orientation relationship and

the nature of the interfacial coherency. Further, such a microstructure with coarse lamellar colonies makes it difficult to activate a large number of independent slip systems. Unlike this situation, in case of the CR700/600 condition, the microstructure is comprised of randomly oriented ~1 µm FCC-based or BCC-based equiaxed grains. Therefore, the average slip length is substantially enhanced in this case as well as the possibility of activating multiple slip systems due to the random orientation of the grains. The details of the deformation mechanisms in both these types of microstructures are the subject of future investigation. Previous reports on classical eutectic systems, such as Ag–Cu, have also reported the synergistic increase in strength and ductility when the microstructure changes from lamellar to equiaxed [23]. Additionally, it also indicates that the multicomponent nature of intermetallic $L1_2$ and B2 phases potentially make them deformable due to a change in their bonding nature, resulting from their complex site occupancies [20]. However, the deformation behavior of these complex intermetallics is the subject of future investigations. The coupled approach involving solution thermodynamic (ThermoCalc) modeling and experimental thermo-mechanical processing, discussed in case of the $Al_{0.3}$CoFeNi CCA/HEA in the present study, led to the design of a novel four-phase hierarchical multi-scale microstructure with an excellent combination of tensile properties.

Conclusions

(1) Using solution thermodynamic modeling (ThermoCalc), a novel four-phase microstructure, comprising FCC, $L1_2$, BCC and B2 phases, has been stabilized in the $Al_{0.3}$CoFeNi CCA/HEA.
(2) Guided by the ThermoCalc modeling, the phase transformation pathways have been engineered via thermo-mechanical processing in this alloy to develop a hierarchical four-phase microstructure, spanning multiple length scales.
(3) The optimized FCC + $L1_2$ + BCC + B2 microstructure in the $Al_{0.3}$CoFeNi CCA/HEA exhibits an excellent combination of high tensile yield stress ~1490 MPa, UTS ~1663 MPa and ductility ~12%.

Acknowledgements

The work was supported by the US Air Force Office of Scientific Research under grant FA9550-17-1-0395. The authors acknowledge the Materials Research Facility (MRF) at the University of North Texas for use of microscopy facilities.

Disclosure statement

No potential conflict of interest was reported by the author(s).

Funding

The work was supported by the US Air Force Office of Scientific Research [grant number FA9550-17-1-0395].

ORCID

S. Gorsse http://orcid.org/0000-0003-1966-8476

References

[1] Vander Voort GF. ASM handbook, volume 9, metallography and microstructures. Materials Park (Ohio): ASM International; 2004.
[2] Cantor B. Multicomponent and high entropy alloys. Entropy. 2014 Aug;16(9):4749–4768.
[3] Yeh JW, Chen SK, Lin SJ, et al. Nanostructured high-entropy alloys with multiple principal elements: novel alloy design concepts and outcomes. Adv Eng Mater. 2004 May;6(5):299–303.
[4] Gwalani B, Gorsse S, Choudhuri D, et al. Modifying transformation pathways in high entropy alloys or complex concentrated alloys via thermo-mechanical processing. Acta Mater. 2018 Jul;153:169–185.
[5] Zhang C, Zhang F, Diao H, et al. Understanding phase stability of Al-Co-Cr-Fe-Ni high entropy alloys. Mater Des. 2016 Nov;109:425–433.
[6] Li Z, Pradeep KG, Deng Y, et al. Metastable high-entropy dual-phase alloys overcome the strength-ductility tradeoff. Nature. 2016 May;534(7606):227–230.
[7] Gwalani B, Gorsse S, Choudhuri D, et al. Tensile yield strength of a single bulk Al0.3CoCrFeNi high entropy alloy can be tuned from 160 MPa to 1800 MPa. Scr Mater. 2019 Mar;162:18–23.
[8] He JY, Wang H, Huang HL, et al. A precipitation-hardened high-entropy alloy with outstanding tensile properties. Acta Mater. 2016 Jan;102:187–196.
[9] Singh S, Wanderka N, Murty BS, et al. Decomposition in multi-component AlCoCrCuFeNi high-entropy alloy. Acta Mater. 2011 Jan;59(1):182–190.
[10] Liang YJ, Wang L, Wen Y, et al. High-content ductile coherent nanoprecipitates achieve ultrastrong high-entropy alloys. Nat Commun. 2018 Dec;9(1):1–8.
[11] Chaudhary V, Gwalani B, Soni V, et al. Influence of Cr substitution and temperature on hierarchical phase decomposition in the AlCoFeNi high entropy alloy. Sci Rep. 2018 Dec;8(1):1–12.
[12] Shaysultanov DG, Salishchev GA, Ivanisenko YV, et al. Novel Fe36Mn21Cr18Ni15Al10high entropy alloy with bcc/B2 dual-phase structure. J Alloys Compd. 2017 May;705:756–763.
[13] Chen C, Zhang H, Fan Y, et al. A novel ultrafine-grained high entropy alloy with excellent combination of mechanical and soft magnetic properties. J Magn Magn Mater. 2020;502:166513.
[14] Sun S, Gao P, Sun G, et al. Nanostructuring as a route to achieve ultra-strong high- and medium-entropy alloys with high creep resistance. J Alloys Compd. 2020;830:154656.

[15] Zhang Y, Zuo TT, Tang Z, et al. Microstructures and properties of high-entropy alloys. Prog Mater Sci. 2014;61:1–93.
[16] Chail G, Kangas P. Super and hyper duplex stainless steels: structures, properties and applications. In: Lacoviello Francesco, Susmel Luca, Ferro Giuseppe, editors. Procedia structural integrity. Catania, Italy: Elsevier B.V.; 2016. p. 1755–1762.
[17] Gwalani B, Gangireddy S, Zheng Y, et al. Influence of ordered L1 2 precipitation on strain-rate dependent mechanical behavior in a eutectic high entropy alloy. Sci Rep. 2019 Dec;9(1):1–13.
[18] Shi P, Ren W, Zheng T, et al. Enhanced strength–ductility synergy in ultrafine-grained eutectic high-entropy alloys by inheriting microstructural lamellae. Nat Commun. 2019 Dec;10(1):1–8.
[19] Qiu Y, Hu YJ, Taylor A, et al. A lightweight single-phase AlTiVCr compositionally complex alloy. Acta Mater. 2017 Jan;123:115–124.
[20] Yang T, Zhao YL, Tong Y, et al. Multicomponent intermetallic nanoparticles and superb mechanical behaviors of complex alloys. Science. 2018 Nov;362(6417):933–937.
[21] Dasari S, Gwalani B, Jagetia A, et al. Hierarchical eutectoid nano-lamellar decomposition in an Al0.3CoFeNi complex concentrated alloy. Sci Rep. 2020 Dec;10(1):1–15.
[22] Langford G. Deformation of pearlite. Metall Trans A. 1977;8:861–875.
[23] Cline HE, Lee D. Strengthening of lamellar vs. equiaxed Ag-Cu eutectic. Acta Metall. 1970.